Research Square

Preprints are preliminary reports that have not undergone peer review.
They should not be considered conclusive, used to inform clinical practice,
or referenced by the media as validated information.

EGCG-Fe-ATV nanocapsules alleviate endothelial inflammation by suppressing TNF-α- mediated cytokine networks

Aiai zhang
The First Affiliated Hospital of Hebei North University
Yue Shi
The First Affiliated Hospital of Hebei North University
Wei Liu
The First Affiliated Hospital of Hebei North University
Jing Yang
Institute of Biomedical Engineering, Chinese Academy of Medical Science & Peking Union Medical College
Feixing Li
The First Affiliated Hospital of Hebei North University
Wei Han
The First Affiliated Hospital of Hebei North University
Wenqing Gao
Central Hospital, Tianjin University/Tianjin Third Central Hospital
Meiling Du
The First Affiliated Hospital of Hebei North University
Kaijing Liu
liukaijing126@126.com

Qingdao Hospital, University of Health and Rehabilitation Sciences (Qingdao Municipal Hospital)

Article

Keywords: Atherosclerosis, Endothelial cells, Transcriptome, TNF signaling pathway, Inflammation

Posted Date: October 7th, 2026

DOI: https://doi.org/10.21203/rs.3.rs-10771706/v1

License: This work is licensed under a Creative Commons Attribution 4.0 International License.
Read Full License

Additional Declarations: Competing interest reported. Competing interests: The authors declare no competing interests.

EGCG-Fe-ATV nanocapsules alleviate endothelial inflammation by suppressing TNF-α-mediated cytokine networks

Aiai Zhang[a], Yue Shi[a], Wei Liu[a], Jing Yang[c], Feixing Li[a], Wei Han[a], Wenqing Gao[d], Meiling Du [a, *], Kaijing Liu [b, *]

a The First Affiliated Hospital of Hebei North University, No.12, Changqing Road, Qiaoxi District, Zhangjiakou City, Hebei 075061, China.

b Qingdao Hospital, University of Health and Rehabilitation Sciences (Qingdao Municipal Hospital), Qingdao 266000, China

c State Key Laboratory of Advanced Medical Materials and Devices, Institute of Biomedical Engineering, Chinese Academy of Medical Science & Peking Union Medical College, Tianjin 300192, China.

d Central Hospital, Tianjin University/Tianjin Third Central Hospital, No.83, Jintang Road, Hedong District, Tianjin 300170, China.

*Corresponding author: Kaijing Liu, Email addresses: liukaijing126@126.com. Meiling Du, Email addresses: raindml@163.com.

Atherosclerosis (AS) is a chronic inflammatory disease initiated by endothelial cell (EC) dysfunction. In our previous study, ROS-responsive EGCG-Fe-ATV nanocapsules were shown to ameliorate atherosclerotic plaque progression in vivo by reshaping the oxidative microenvironment. However, the transcriptome-wide regulatory mechanisms of EGCG-Fe-ATV in ECs remain elusive.In this study, a phorbol 12-myristate 13-acetate (PMA)-induced human umbilical vein endothelial cell (HUVEC) inflammation model was established and treated with EGCG-Fe-ATV. RNA sequencing (RNA-seq) was performed to profile gene expression changes, followed by KEGG and GO enrichment analyses. Protein-protein interaction (PPI) networks were constructed to identify hub genes. Key inflammatory mediators were validated by quantitative real-time PCR (qPCR) and Western blot (WB).RNA-seq identified 508 differentially expressed genes (DEGs) between PMA-stimulated ECs and EGCG-Fe-ATV-treated ECs, with 375 genes downregulated and 133 upregulated. KEGG analysis revealed significant enrichment in the TNF signaling pathway, cytokine-cytokine receptor interaction, NF-kappa B signaling pathway, and cell cycle regulation. Among 81 overlapping DEGs across Normal, Control, and Treated groups, the TNF signaling pathway and

cytokine-mediated signaling were the most significantly enriched biological processes. PPI network analysis identified MMP9, CXCL1, and VCAM1 as central hub genes. qPCR and WB further confirmed that EGCG-Fe-ATV significantly suppressed the expression of CXCL1, VCAM1, MMP9, IL-6, and IL-1β at both transcriptional and translational levels.Our findings demonstrate that EGCG-Fe-ATV alleviates endothelial inflammatory activation primarily by suppressing the TNF-α/NF-κB-driven cytokine network, highlighting its potential as a nanotherapeutic strategy for atherosclerosis.

Keyword: Atherosclerosis; Endothelial cells; Transcriptome; TNF signaling pathway; Inflammation

Atherosclerosis (AS) remains the leading cause of cardiovascular morbidity and mortality worldwide, characterized by lipid-rich plaque formation in the intima of large and medium-sized arteries, accompanied by immune cell infiltration and extracellular matrix remodeling[1, 2]. Despite significant reductions in cardiovascular mortality achieved through lifestyle interventions and lipid-lowering therapies over the past three decades, conventional pharmacological strategies—most notably statins and anticoagulants—are constrained by limited bioavailability, prolonged treatment duration, and systemic off-target effects[3, 4]. Because these agents distribute non-specifically throughout the body, they often fail to achieve therapeutic concentrations within atherosclerotic plaques while causing unwanted side effects in non-target tissues[5]. Consequently, there is an urgent clinical need for targeted therapeutic platforms that can precisely modulate plaque microenvironment with improved efficacy and safety profiles.

Nanomaterial-based drug delivery systems have emerged as transformative tools in atherosclerosis management, offering surface modifiability, enhanced targeting capability, and reduced systemic toxicity[4-6]. Among these, metal-phenolic frameworks (MPFs) constructed from natural polyphenols and metal ions have attracted considerable attention due to their excellent biocompatibility, intrinsic antioxidant capacity, and stimuli-responsive degradability[7, 8]. In our previous study, we engineered ROS-responsive EGCG-Fe-ATV nanocapsules by coordinating epigallocatechin gallate (EGCG) with Fe^{3+} to form a metal-phenolic network, into which atorvastatin (ATV) was encapsulated[9]. This nanosystem demonstrated favorable ROS-scavenging capacity, sustained intracellular drug release, and significant therapeutic efficacy in

ApoE$^{-/-}$ mice, as evidenced by reduced aortic plaque burden, attenuated inflammatory cell infiltration, and improved lipid profiles[9]. Notably, the dual-action design—combining EGCG-mediated ROS neutralization with ATV-dependent lipid regulation—positions this platform as a multi-modal nanotherapeutic. However, the cellular and transcriptome-wide mechanisms by which EGCG-Fe-ATV modulates endothelial function, particularly its effects on inflammatory gene networks, remain largely unexplored.

Endothelial dysfunction, driven by chronic inflammation and oxidative stress, represents the initiating event in atherogenesis[10]. Upon exposure to inflammatory stimuli, endothelial cells (ECs) upregulate adhesion molecules (e.g., VCAM1), chemokines (e.g., CXCL1), and matrix metalloproteinases (e.g., MMP9), which collectively promote monocyte adhesion, transmigration, and subsequent foam cell formation[11]. While prior work established the in vivo efficacy of EGCG-Fe-ATV, the precise transcriptional reprogramming events occurring at the endothelial interface—the primary barrier between circulating inflammatory mediators and the vascular wall—have yet to be systematically characterized. Transcriptomic profiling via RNA sequencing (RNA-seq) provides an unbiased, high-resolution approach to dissecting the complex gene regulatory networks underlying nanotherapeutic action[12]. Unlike conventional single-pathway assays, RNA-seq can simultaneously capture the integrated effects of drug, carrier, and their emergent biological properties, enabling the identification of core signaling axes and hub genes that drive pathological processes.

In the present study, we employed a PMA-induced human umbilical vein endothelial cell (HUVEC) inflammation model to investigate the transcriptomic landscape of EGCG-Fe-ATV treatment. Our aims were to (i) characterize the global gene expression changes elicited by EGCG-Fe-ATV in activated ECs, (ii) identify the core signaling pathways and hub genes associated with its anti-inflammatory effects through KEGG, GO, and protein-protein interaction (PPI) network analyses, and (iii) validate key downstream targets using quantitative real-time PCR (qPCR) and Western blot. Our results reveal that EGCG-Fe-ATV predominantly suppresses TNF-α-mediated cytokine signaling and NF-κB-related inflammatory networks in ECs, establishing a mechanistic link between ROS-responsive nanocapsule disassembly and endothelial protective effects.

Results

Biosafety and Cellular Internalization

To establish the experimental premise for transcriptomic analysis, the biosafety and cellular uptake profile of EGCG-Fe-ATV in HUVECs were evaluated. As illustrated in Fig. 1A, EGCG-Fe-ATV nanocapsules were constructed via metal–phenolic coordination between EGCG and Fe^{3+}, with ATV encapsulated within the hollow cavity[9]. In the extracellular physiological environment (pH 7.4), the nanocapsules maintain structural integrity with minimal ATV leakage. Upon internalization into the intracellular ROS-rich microenvironment, the EGCG–Fe coordination bonds are cleaved, triggering accelerated ATV release and simultaneous ROS scavenging by the liberated EGCG phenolic hydroxyl groups.

Cell viability was assessed by CCK-8 assay following 24 h exposure to EGCG-Fe-ATV at concentrations ranging from 12.5 to 200 μg/mL. As shown in Fig. 1B, no significant cytotoxicity was observed across the entire concentration range, with cell viability remaining above 95% relative to the untreated control (all $P > 0.05$, ns). These results confirm the excellent biocompatibility of EGCG-Fe-ATV in endothelial cells, consistent with our previous findings in smooth muscle cells, macrophages, and fibroblasts[9].

To determine whether HUVECs could efficiently internalize the nanocapsules, we performed confocal laser scanning microscopy using coumarin-6-loaded EGCG-Fe nanocapsules (EGCG-Fe-Coumarin). Free coumarin-6 exhibited negligible intracellular fluorescence at both 1 h and 3 h (Fig. 1C, top two rows), indicating poor passive diffusion across the endothelial membrane. In stark contrast, cells treated with EGCG-Fe-Coumarin displayed bright punctate green fluorescence in the cytoplasm at 1 h, which further intensified and became more diffusely distributed by 3 h (Fig. 1C, bottom two rows). The merged images confirmed successful time-dependent internalization and perinuclear accumulation of the nanocapsules. Collectively, these data demonstrate that the EGCG-Fe metal – phenolic framework not only ensures biosafety but also markedly enhances cargo delivery into HUVECs, providing a robust basis for subsequent transcriptomic interrogation of its anti-inflammatory mechanisms.

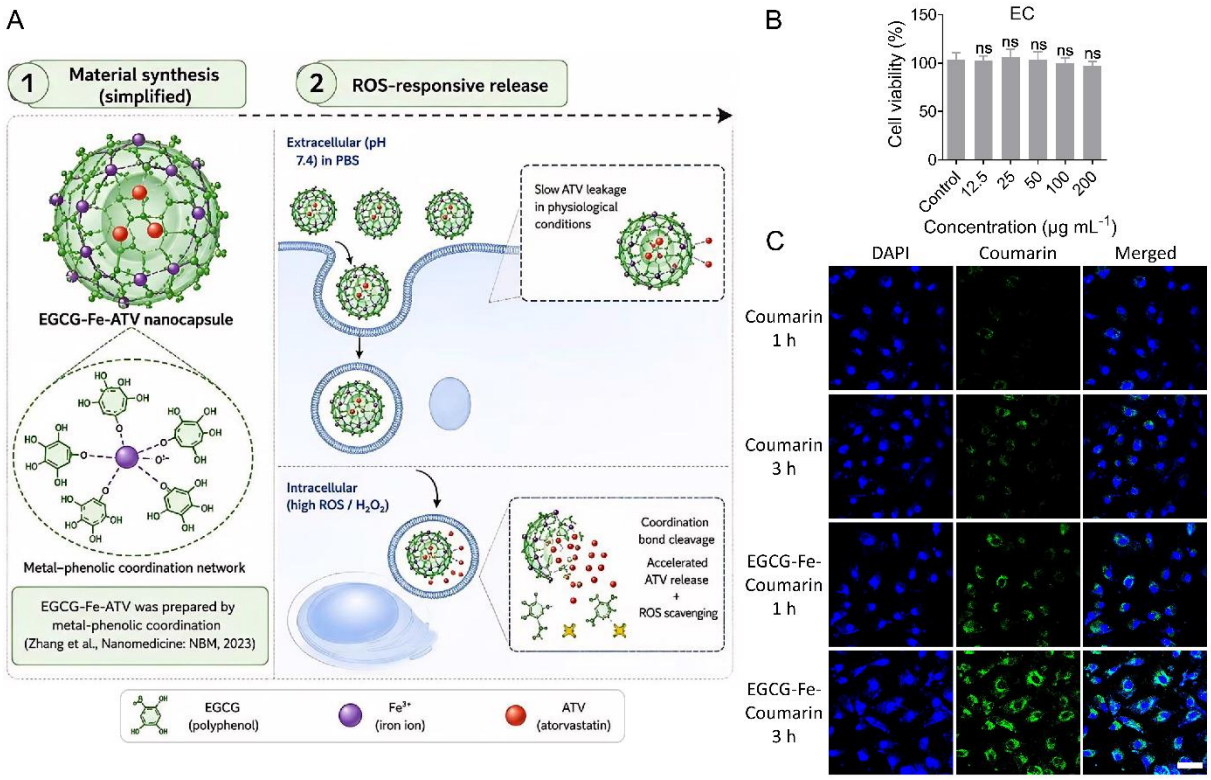


Figure 1. Biosafety and ROS-responsive cellular internalization of EGCG-Fe-ATV in HUVECs. (A) Schematic illustration of EGCG-Fe-ATV nanocapsule structure, metal–phenolic coordination network, and ROS-responsive intracellular drug release. In the extracellular physiological environment (pH 7.4), the nanocapsule maintains structural integrity with slow ATV leakage; upon internalization into the intracellular ROS-rich milieu, the EGCG–Fe coordination bonds are cleaved, resulting in accelerated ATV release and concurrent ROS scavenging. (B) CCK-8 assay demonstrating the viability of HUVECs treated with increasing concentrations of EGCG-Fe-ATV (12.5–200 μg/mL) for 24 h. Data are presented as mean ± SD (n = 3; ns, not significant versus Control). (C) Confocal laser scanning microscopy images showing cellular uptake of free coumarin-6 (top two rows) and EGCG-Fe-Coumarin (bottom two rows) in HUVECs at 1 h and 3 h. Blue: DAPI (nucleus); Green: coumarin-6. Scale bar = 50 μm.

Global Transcriptomic Landscape and Pathway Enrichment

To systematically dissect the molecular mechanisms underlying EGCG-Fe-ATV action in activated endothelial cells, we performed transcriptomic profiling of HUVECs across three experimental conditions: Normal, PMA-stimulated Control, and EGCG-Fe-ATV-treated

(Treated). High-quality sequencing data were obtained for all samples, with Q20 > 98% and Q30 > 93% (Table 1).

Table 1 Quality control metrics of RNA-seq data.

EC Sample	Total Raw Reads (M)	Total Clean Reads (M)	Total Clean Bases (Gb)	Clean Reads Q20 (%)	Clean Reads Q30 (%)	Clean Reads Ratio (%)
control1	24.47	22.21	6.66	98.4	94.53	90.76
control2	23.59	22.4	6.72	98.05	93.31	94.96
control3	23.59	22.27	6.68	98.06	93.33	94.4
normal1	23.59	22.04	6.61	98.37	94.32	93.43
normal2	23.59	21.99	6.6	98.12	93.47	93.22
normal3	23.59	22.35	6.7	98.17	93.74	94.74
treated1	23.59	22.44	6.73	98.19	93.84	95.13
treated2	23.59	22.29	6.69	98.12	93.59	94.49
treated3	19.94	18.98	5.69	98.22	93.88	95.19

Comparative analysis between the Control and Treated groups identified 508 differentially expressed genes (DEGs), with stringent thresholds of $|\log_2(\text{fold change})| \geqslant 1$ and q-value $\leqslant$ 0.05. Notably, the vast majority of DEGs were downregulated (375 genes, 73.8%) rather than upregulated (133 genes, 26.2%), as visualized in the volcano plot (Fig. 2A). This asymmetric transcriptional suppression pattern suggests that EGCG-Fe-ATV primarily functions by dampening the aberrant gene activation program induced by PMA, rather than broadly inducing de novo transcriptional responses.

KEGG pathway enrichment analysis of the 508 DEGs revealed a striking predominance of inflammation- and proliferation-related pathways (Fig. 2B). The TNF signaling pathway ranked as the most significantly enriched term, followed by the IL-17 signaling pathway, NF-kappa B signaling pathway, and cytokine-cytokine receptor interaction. Additionally, cell cycle regulation, Fanconi anemia pathway, and homologous recombination were prominently

represented, indicating that EGCG-Fe-ATV concurrently modulates endothelial inflammatory signaling and proliferative responses.

Heatmap visualization of the top enriched pathways demonstrated clear segregation between the Control and Treated groups (Fig. 2C). In the cell cycle cluster, key mitotic regulators—including CCNA1, CCNB1, CCNB2, PLK1, ESPL1, and CDC20—were markedly elevated in the Control group and suppressed following EGCG-Fe-ATV treatment. In the TNF signaling pathway cluster, pro-inflammatory mediators such as IL1B, IL6, CXCL1, CXCL2, CXCL5, CXCL6, PTGS2, and SELE exhibited robust downregulation in the Treated group. Similarly, the cytokine-cytokine receptor interaction cluster revealed coordinated suppression of CXCL12, CSF2, CSF3, TNFSF15, IL33, INHBA, and CCL2. These expression patterns collectively indicate that EGCG-Fe-ATV attenuates EC activation by suppressing chemokine production, cytokine signaling, and cell cycle progression.

GO biological process (GO-BP) enrichment analysis further corroborated these findings (Fig. 2D). The top enriched terms included cell division, mitotic spindle organization, chromosome segregation, and mitotic cell cycle, consistent with the KEGG cell cycle pathway enrichment. Importantly, chemokine-mediated signaling pathway, chemotaxis, and DNA repair also ranked among the significantly enriched biological processes, reinforcing the dual impact of EGCG-Fe-ATV on inflammatory signaling and genomic stability. GO molecular function (GO-MF) analysis highlighted microtubule binding, chemokine activity, heparin binding, and ATP-dependent microtubule motor activity (Fig. S1A), while GO cellular component (GO-CC) analysis revealed enrichment in chromosome, centromeric region, spindle pole, and extracellular space (Fig. S1B). These results collectively indicate that EGCG-Fe-ATV targets both intracellular mitotic machinery and extracellular inflammatory mediators.

Finally, we examined the DNA repair pathway in greater detail, as oxidative stress-induced DNA damage is a hallmark of endothelial dysfunction in atherosclerosis. As shown in Fig. 2E, key DNA repair genes—including POLQ, NEIL3, BRCA1, BRCA2, FANCA, RAD51, and RAD54L—were downregulated in the Treated group relative to the Control. While this downregulation may reflect reduced cellular stress and consequently diminished demand for DNA repair machinery, the precise functional implications warrant further investigation.

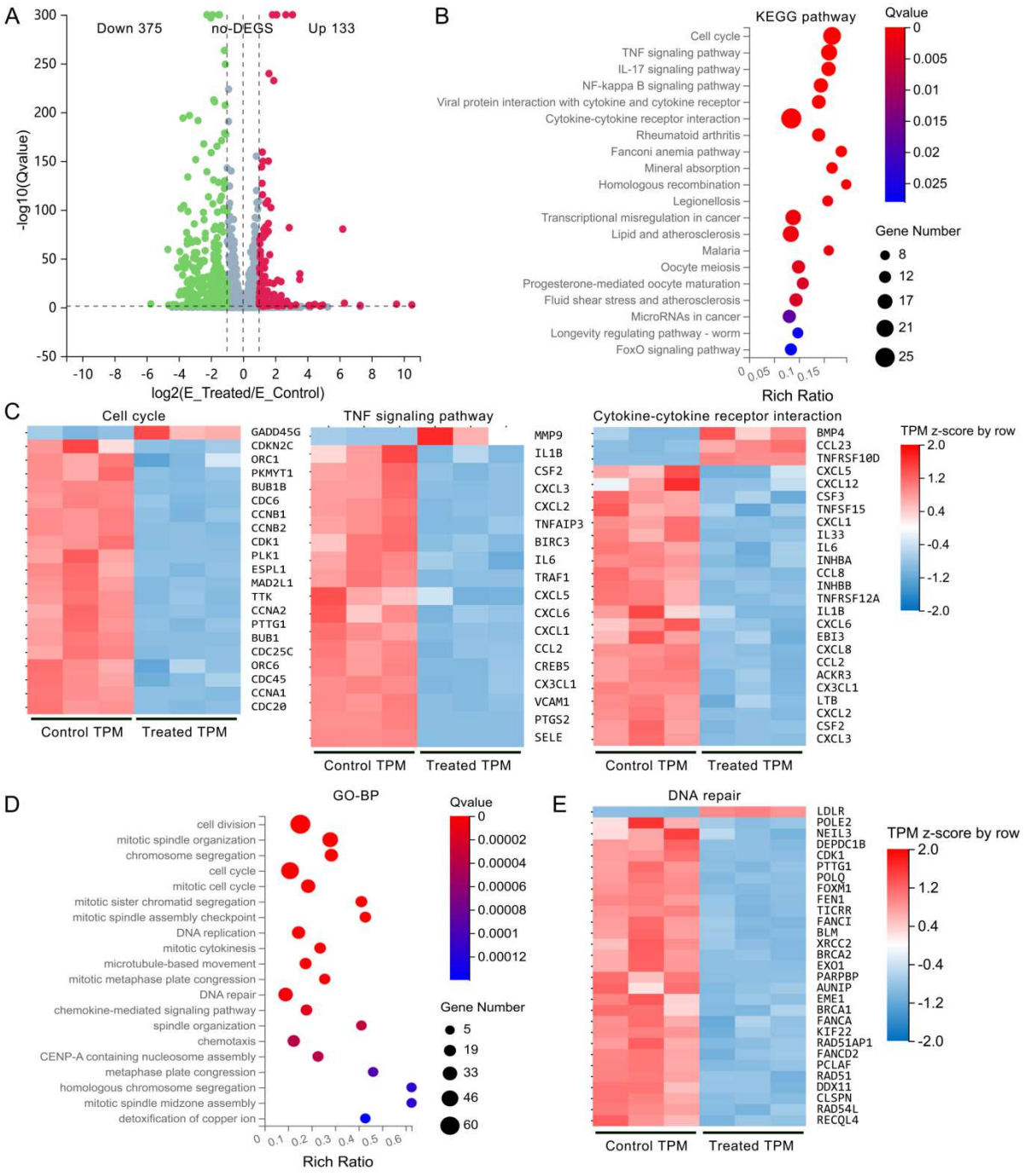


Figure 2. Global transcriptomic profiling reveals that EGCG-Fe-ATV suppresses inflammatory and proliferative gene programs in PMA-stimulated HUVECs. (A) Volcano plot depicting 508 DEGs between Control and Treated groups. Green: downregulated genes (n = 375); Magenta: upregulated genes (n = 133); Gray: non-significant genes. (B) KEGG pathway enrichment analysis of the 508 DEGs. Bubble color represents q-value; bubble size represents gene number. (C) Heatmaps showing row z-score normalized expression of DEGs within the Cell cycle, TNF signaling pathway, and Cytokine-cytokine receptor interaction pathways. (D) GO biological process enrichment analysis of the 508 DEGs. (E) Heatmap showing row z-score normalized

expression of DEGs within the DNA repair pathway.

Core Inflammatory Network Analysis of Overlapping DEGs

To identify genes consistently regulated across the entire experimental spectrum (from normal homeostasis to inflammatory activation and subsequent therapeutic intervention), we analyzed the 81 overlapping DEGs among the Normal, Control, and Treated groups (Fig. 3A). KEGG enrichment analysis of these core genes confirmed significant enrichment in the TNF signaling pathway and cytokine-cytokine receptor interaction (Fig. 3B), reinforcing the centrality of TNF-α-driven inflammation in the EC response to EGCG-Fe-ATV.

Heatmap analysis of the 81 genes revealed robust expression changes in TNF signaling components, including MMP9, CXCL6, CXCL1, CX3CL1, and VCAM1, all of which were elevated in the Control group and restored toward normal levels upon EGCG-Fe-ATV treatment (Fig. 3C). Similarly, in the cytokine-cytokine receptor interaction pathway, CCL23, TNFRSF12A, CXCL1, CX3CL1, IL33, CXCL6, and TNFSF15 showed comparable expression patterns (Fig. 3D). The cytokine-mediated signaling pathway also exhibited downregulation of SDC1, CXCL1, CX3CL1, VCAM1, SOCS1, NOS2, MMP9, and CRLF1 in the Treated group (Fig. 3E).

GO-BP analysis of the 81 overlapping genes identified chemotaxis, cytokine-mediated signaling pathway, regulation of chemokine production, and endothelium development as significantly enriched terms (Fig. 3F). GO-MF analysis highlighted chemokine activity, heparin binding, calmodulin binding, and integrin binding (Fig. S2A), while GO-CC analysis pointed to extracellular space, extracellular region, and plasma membrane (Fig. S2B), consistent with the secretory and membrane-bound nature of inflammatory mediators.

PPI network construction based on the 81 core genes revealed a densely connected inflammatory network with MMP9 and CXCL1 serving as central hub nodes (Fig. 3G). MMP9 exhibited the highest degree of connectivity, interacting directly with CXCL1, NOS2, VCAM1, CX3CL1, and CXCL6. These hub genes represent critical convergence points in the EC inflammatory response and likely constitute key effectors of EGCG-Fe-ATV-mediated protection.

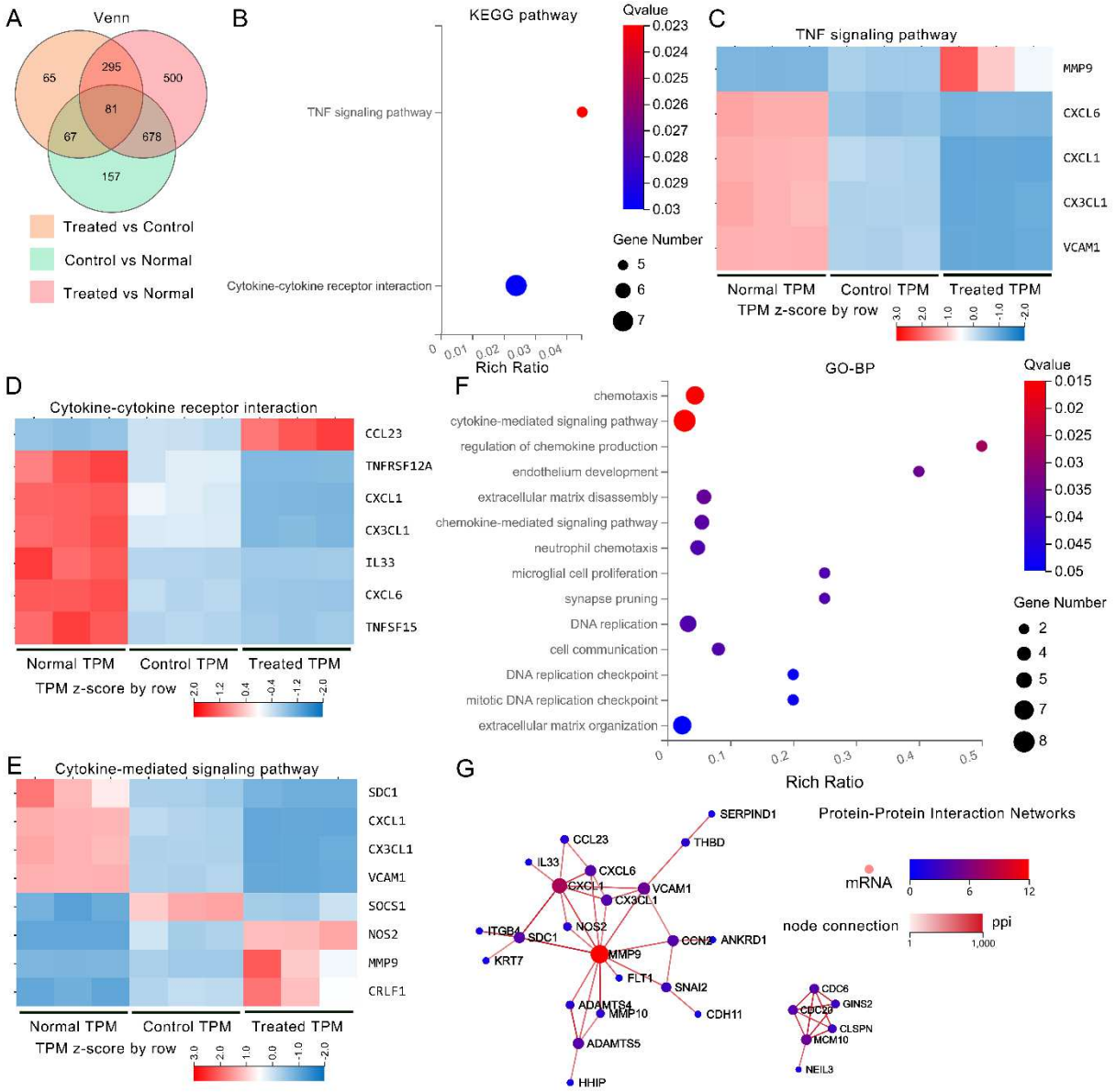


Figure 3. Core inflammatory network analysis of 81 overlapping DEGs among Normal, Control, and Treated groups. (A) Venn diagram showing the overlap of DEGs. (B) KEGG pathway enrichment analysis of the 81 overlapping genes. (C-E) Heatmaps of differentially expressed genes in the TNF signaling pathway (C), Cytokine-cytokine receptor interaction (D), and Cytokine-mediated signaling pathway (E). (F) GO biological process enrichment analysis of the 81 overlapping genes. (G) Protein-protein interaction network constructed from the 81 overlapping genes. Node size represents connectivity degree; node color represents log2 fold change.

Molecular Validation of Key Inflammatory Mediators

To confirm the transcriptomic findings, we validated the expression of five hub inflammatory genes—CXCL1, VCAM1, MMP9, IL-6, and IL-1β—using qPCR and Western blot. As shown in Fig. 4A, PMA stimulation significantly upregulated the mRNA levels of all five target genes compared to the Normal group ($P < 0.001$). EGCG-Fe-ATV treatment markedly attenuated these elevations, with CXCL1, VCAM1, MMP9, IL-6, and IL-1β all showing significant downregulation relative to the Control group ($P < 0.01$ or $P < 0.001$). Full-length uncropped images were provided in Figure S3.

Western blot analysis corroborated the qPCR results at the protein level (Fig. 4B and 4C). PMA stimulation induced robust protein expression of CXCL1, VCAM1, MMP9, IL-6, and IL-1β, whereas EGCG-Fe-ATV treatment significantly suppressed the expression of all five proteins. Quantitative densitometric analysis confirmed that protein levels in the Treated group were restored to levels comparable to or lower than the Normal group. The concordance between RNA-seq, qPCR, and WB data establishes CXCL1, VCAM1, MMP9, IL-6, and IL-1β as bona fide downstream targets of EGCG-Fe-ATV in activated ECs.

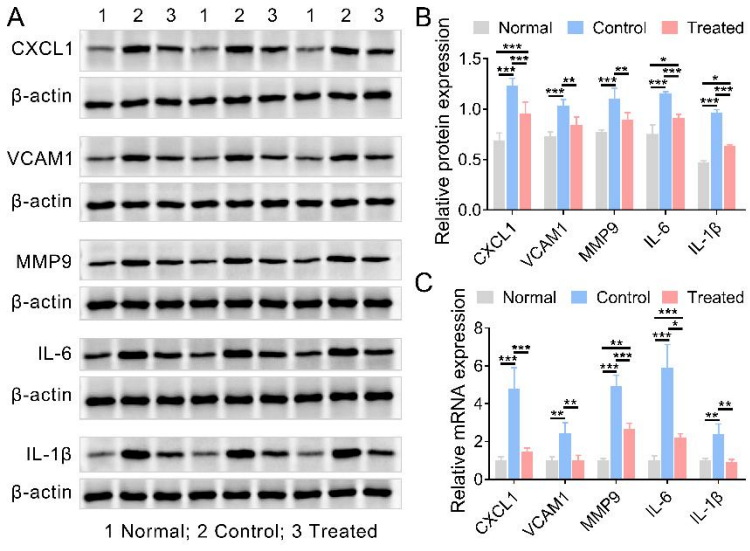


Figure 4. Molecular validation of key inflammatory mediators. (A) Relative mRNA expression of CXCL1, VCAM1, MMP9, IL-6, and IL-1β determined by qPCR. (B) Representative Western blot bands for CXCL1, VCAM1, MMP9, IL-6, IL-1β, and β-actin. (C) Quantitative densitometric analysis of Western blot results. Data are presented as mean ± SD ($n = 3$). $P <$

0.05, P < 0.01, P < 0.001, ****P < 0.0001.

Discussion

Atherosclerosis is fundamentally an inflammatory disease of the arterial wall, and endothelial dysfunction represents the earliest detectable abnormality in this pathological cascade[13]. The present study provides the first transcriptome-wide characterization of EGCG-Fe-ATV action in HUVECs, revealing that this metal-phenolic nanocapsule system alleviates endothelial inflammatory activation primarily through suppression of the TNF-α-mediated cytokine network and NF-κB-related signaling pathways.

Our RNA-seq analysis identified 508 DEGs in PMA-stimulated ECs following EGCG-Fe-ATV treatment, with a striking predominance of downregulated genes (375 vs. 133 upregulated). This transcriptional suppression pattern aligns with the drug's anti-inflammatory function, suggesting that EGCG-Fe-ATV counteracts the broad gene activation program triggered by inflammatory stimuli. KEGG enrichment analysis pinpointed the TNF signaling pathway, cytokine-cytokine receptor interaction, and NF-kappa B signaling pathway as the top enriched terms among the DEGs. These pathways are well-established drivers of EC activation, governing the expression of adhesion molecules, chemokines, and matrix-degrading enzymes that facilitate leukocyte recruitment and plaque destabilization[14].

The 81 overlapping DEGs across Normal, Control, and Treated groups provided a refined dataset of "core response genes" whose expression trajectories are consistently modulated by both inflammation and therapeutic intervention. KEGG and GO analyses of this subset reinforced the dominance of TNF signaling and cytokine-mediated processes. Notably, the PPI network identified MMP9 and CXCL1 as the most highly connected hub genes. MMP9 is a gelatinase that degrades basement membrane collagen and elastin, promoting both leukocyte transmigration and fibrous cap thinning in advanced plaques[15, 16]. CXCL1 is a potent neutrophil chemoattractant that amplifies inflammatory cascades within the arterial wall[17]. The central positioning of these genes in the interaction network underscores their importance as effector molecules in EGCG-Fe-ATV's anti-atherosclerotic mechanism.

Our molecular validation experiments confirmed that EGCG-Fe-ATV significantly downregulates CXCL1, VCAM1, MMP9, IL-6, and IL-1β at both mRNA and protein levels. Each of these targets carries distinct pathophysiological relevance in atherosclerosis. VCAM1

mediates the firm adhesion of monocytes and T cells to activated endothelium, representing a critical checkpoint in early lesion formation[18]. IL-6 and IL-1β are canonical pro-inflammatory cytokines that sustain systemic and local inflammation, with clinical trials demonstrating that IL-1β inhibition reduces cardiovascular event rates[19, 20]. The coordinated suppression of these mediators by EGCG-Fe-ATV suggests a multi-node intervention strategy that disrupts the EC-inflammatory cell communication axis.

The mechanism underlying these transcriptional changes likely involves the ROS-responsive properties of the EGCG-Fe framework. PMA-induced EC activation is accompanied by robust NADPH oxidase activation and mitochondrial ROS generation, which in turn activate redox-sensitive transcription factors including NF-κB. Upon nuclear translocation, NF-κB p65 binds to promoter regions of target genes such as VCAM1, CXCL1, IL-6, and MMP9, driving their transcription. EGCG, as a major constituent of the nanocapsule shell, possesses potent ROS-scavenging capacity and has been shown to inhibit IκB kinase activity, thereby preventing NF-κB nuclear translocation[21]. Additionally, the sustained release of ATV from the nanocapsules may contribute to anti-inflammatory effects through statin-mediated inhibition of isoprenoid synthesis and RhoA signaling, which further suppresses NF-κB activation[22]. Although the present study did not directly assess NF-κB p65 phosphorylation or nuclear translocation, the significant enrichment of the NF-kappa B signaling pathway among the DEGs, combined with the observed downregulation of its downstream targets, strongly supports this mechanistic model. Future studies incorporating NF-κB reporter assays and p65 immunofluorescence will be essential to definitively establish this regulatory axis.

This study connects our previous in vivo findings with cellular-level mechanisms. In ApoE$^{-/-}$ mice, EGCG-Fe-ATV reduced serum IL-6, TNF-α, and IL-1β levels, decreased aortic plaque area, and stabilized lesions[9]. The present data demonstrate that these systemic anti-inflammatory effects are at least partially attributable to direct suppression of EC inflammatory gene expression. By downregulating VCAM1 and CXCL1, EGCG-Fe-ATV likely reduces monocyte and neutrophil recruitment to the nascent plaque, while MMP9 suppression may limit extracellular matrix degradation and plaque vulnerability. Thus, the nanocapsule system acts at the very inception of the atherosclerotic cascade—endothelial activation—to interrupt disease progression.

Several limitations should be acknowledged. First, this study relied on a single in vitro inflammatory model (PMA-stimulated HUVECs); additional validation using TNF-α or LPS stimulation, as well as flow-based shear stress models, would strengthen the generalizability of our findings. Second, while our transcriptomic and molecular data strongly implicate the TNF/NF-κB axis, direct evidence of NF-κB p65 phosphorylation, IκBα degradation, and nuclear translocation was not obtained and should be addressed in future work. Third, functional assays such as monocyte adhesion to EC monolayers were not performed; given the marked VCAM1 and CXCL1 downregulation, such experiments would provide important functional confirmation of the transcriptomic findings.

Conclusion

In conclusion, this study employs integrated transcriptomic and molecular analyses to elucidate the protective mechanisms of EGCG-Fe-ATV nanocapsules in endothelial cells. Our findings demonstrate that EGCG-Fe-ATV suppresses PMA-induced EC activation by downregulating TNF-α-mediated cytokine signaling and inhibiting the expression of key inflammatory mediators including CXCL1, VCAM1, MMP9, IL-6, and IL-1β. These results establish a mechanistic link between the nanocapsule's ROS-responsive drug delivery and its atheroprotective effects, supporting the continued development of EGCG-Fe-ATV as a targeted nanotherapeutic for atherosclerosis.

Materials and Methods

Materials

The synthesis and characterization of EGCG-Fe-ATV nanocapsules were performed as previously described[9]. Briefly, a ZIF-8 or ZIF-8-ATV template was first prepared, followed by surface coating with an EGCG-Fe coordination layer. After EDTA-mediated template removal, hollow EGCG-Fe or EGCG-Fe-ATV nanocapsules were obtained. The hydrodynamic diameter, zeta potential, morphology, and ROS-responsive ATV release behavior were confirmed in our prior work[9]. Human umbilical vein endothelial cells (HUVECs) and endothelial cell medium were purchased from iCell Bioscience Inc. (Shanghai, China). Phorbol 12-myristate 13-acetate (PMA) was obtained from Sigma-Aldrich (USA).

Cell Culture and Treatment

HUVECs were cultured in endothelial cell medium supplemented with 10% fetal bovine serum

(FBS) and 1% penicillin-streptomycin at 37 °C in a humidified atmosphere containing 5% CO_2. Cells at passages 3–6 were used for experiments. To establish the inflammatory model, HUVECs were stimulated with PMA (10 μM) for 24 h. For the treatment group, cells were treated with PMA and EGCG-Fe-ATV (50 μg/mL) for 24 h. The experimental groups were defined as follows: Normal (untreated), Control (PMA alone), and Treated (PMA + EGCG-Fe-ATV).

Cell Viability Assay

Cell viability was assessed using the Cell Counting Kit-8 (CCK-8) assay. HUVECs were seeded in 96-well plates at a density of 5,000 cells per well and incubated for 24 h. Subsequently, cells were treated with various concentrations of EGCG-Fe-ATV (0, 12.5, 25, 50, 100, 200 μg/mL) for 24 h. CCK-8 solution (10 μL) was added to each well, and the plates were incubated for 30 min. Absorbance was measured at 450 nm using a microplate reader. Cell viability was expressed as a percentage relative to the untreated control.

Cellular Uptake Analysis

To visualize cellular internalization, coumarin-6 was encapsulated into EGCG-Fe nanocapsules (EGCG-Fe-Coumarin) using the same protocol as for EGCG-Fe-ATV preparation, substituting ATV with coumarin-6. HUVECs were seeded in confocal dishes at a density of 5×10^4 cells per well and cultured for 24 h. EGCG-Fe-Coumarin or free coumarin-6 (equivalent coumarin concentration) was added and incubated for 1 h or 3 h. Cells were then washed three times with PBS, fixed with 4% paraformaldehyde for 15 min, and stained with DAPI (1 μg/mL) for 5 min. Cellular uptake was observed using a confocal laser scanning microscope (CLSM).

RNA Sequencing and Bioinformatics Analysis

Total RNA was extracted from Normal, Control, and Treated HUVECs (n = 3 per group) using TRIzol reagent. RNA quality was assessed using a NanoDrop spectrophotometer and Agilent Bioanalyzer 2100. Strand-specific RNA-seq libraries were constructed and sequenced on the DNBSEQ platform (BGI, Wuhan, China) with paired-end 150 bp reads. Raw reads were filtered to remove adapter sequences, low-quality reads, and rRNA contamination. Clean reads were aligned to the human reference genome (GRCh38) using HISAT2. Gene expression levels were quantified as fragments per kilobase of transcript per million mapped reads (FPKM) using RSEM.

Differential expression analysis was performed using DESeq2. Genes with $|\log_2(\text{fold change})| \geqslant 1$ and q-value $\leqslant 0.05$ were defined as differentially expressed genes (DEGs). KEGG pathway enrichment[23, 24] and GO functional enrichment analyses were conducted using clusterProfiler. A hypergeometric test was applied, and q-values were corrected using the Benjamini-Hochberg method. Significantly enriched pathways were identified at $q < 0.05$. PPI networks were constructed using the STRING database and visualized in Cytoscape. Hub genes were identified based on node degree connectivity.

Western Blot Analysis

Cells were lysed in RIPA buffer containing protease and phosphatase inhibitors. Protein concentrations were determined using the BCA assay. Equal amounts of protein (20 μg per lane) were separated by 10% SDS-PAGE and transferred to PVDF membranes. After blocking with 5% non-fat milk for 1 h, membranes were incubated overnight at 4 °C with primary antibodies against CXCL1, VCAM1, MMP9, IL-6, IL-1β, and β-actin (1:1000 dilution). After washing, membranes were incubated with HRP-conjugated secondary antibodies for 1 h at room temperature. Protein bands were visualized using an ECL chemiluminescence kit and quantified using ImageJ software. For CXCL1, the immunoblotting and loading control were obtained from the same gel or membrane and were cut out separately. For VCAM1, MMP9, IL-6, and IL-1β, membranes were probed for the target protein, then stripped and re-probed for β-actin. Full-length uncropped images are provided in Figure S3.

Quantitative Real-Time PCR (qPCR)

Total RNA was reverse-transcribed into cDNA using a PrimeScript RT Reagent Kit. qPCR was performed using SYBR Green Master Mix on a QuantStudio 3 Real-Time PCR system. The relative expression levels of target genes were normalized to GAPDH and calculated using the $2^{-\Delta\Delta Ct}$ method.

Fragments Sequence.

CXCL1	F:ctgggattcacctcaagaacatc	R: cagggtcaaggcaagcctc
VCAM1	F:gctgacatgcgtggtgatcg	R: caggtagcgttggaaccggt
MMP9	F:cagaggtaacccacgtcagc	R: gggatccaccttctgagactt
IL-6	F:tagtccttcctaccccaatttcc	R: ttggtccttagccactccttc
IL-1β	F:ttcaggcaggcagtatcactc	R: gaaggtccacgggaaagacac.

Statistical Analysis

Data are presented as mean ± standard deviation (SD) from at least three independent experiments. Statistical significance was determined using one-way ANOVA followed by Tukey's post-hoc test. A P-value < 0.05 was considered statistically significant ($P < 0.05$, $P < 0.01$, $P < 0.001$, ****$P < 0.0001$).

Data availability

The transcriptome RNA-seq data generated in this study have been deposited in NCBI under BioProject accession PRJNA1520836 and SRA Study accession SRP731694. The BioSample accessions are SAMN62781120–SAMN62781128, and the SRA Run accessions are SRR40412282–SRR40412290.

https://dataview.ncbi.nlm.nih.gov/object/PRJNA1520836?reviewer=c8jkh7f4ibb8k6tglfmt5p1foj. These proteins are detailed in Supplementary Table, which is provided as part of the supplementary materials for this manuscript.

References

1. Henein, M.Y., Vancheri, S., Longo, G. & Vancheri, F. The Role of Inflammation in Cardiovascular Disease. *International Journal of Molecular Sciences* **23**, 12906 (2022).
2. Engelen, S.E., Robinson, A.J.B., Zurke, Y.-X. & Monaco, C. Therapeutic strategies targeting inflammation and immunity in atherosclerosis: how to proceed? *Nature Reviews Cardiology* **19**, 522-542 (2022).
3. Golledge, J. Update on the pathophysiology and medical treatment of peripheral artery disease. *Nature Reviews Cardiology* **19**, 456-474 (2022).
4. Tong, J. et al. Advanced Applications of Nanomaterials in Atherosclerosis Diagnosis and Treatment: Challenges and Future Prospects. *ACS Applied Materials & Interfaces* **16**, 58072-58099 (2024).
5. Li, W., Gonzalez, K.M., Chung, J., Kim, M. & Lu, J. Surface-modified nanotherapeutics targeting atherosclerosis. *Biomaterials Science* **10**, 5459-5471 (2022).
6. Perera, B., Wu, Y., Nguyen, N.-T. & Ta, H.T. Advances in drug delivery to atherosclerosis: Investigating the efficiency of different nanomaterials employed for different type of drugs. *Materials Today Bio* **22**, 100767 (2023).
7. Qin, J., Guo, N., Yang, J. & Chen, Y. in Biosensors, Vol. 13 776 (2023).
8. Li, M. et al. Multifunctional Metal–Phenolic Networks: A Game-Changer in Food Preservation Technologies. *Comprehensive Reviews in Food Science and Food Safety* **24**, e70293 (2025).
9. Zhang, A. et al. Metal-phenolic capsules with ROS scavenging reshape the oxidative microenvironment of atherosclerosis. *Nanomedicine: Nanotechnology, Biology and Medicine* **53**, 102700 (2023).
10. Higashi, Y. in Antioxidants, Vol. 11 1958 (2022).

11. Jiang, Y. et al. The calcium-sensing receptor alleviates endothelial inflammation in atherosclerosis through regulation of integrin β1-NLRP3 inflammasome. *The FEBS Journal* **292**, 191-205 (2025).
12. Nuanpirom, J. & Charoensawan, V. Multimodal bioinformatic analyses of genome-scale expression beyond gene-centric differential expression. *Briefings in Bioinformatics* **27**, bbag152 (2026).
13. Deng, Y. et al. pH-sensitive nano-drug delivery systems dual-target endothelial cells and macrophages for enhanced treatment of atherosclerosis. *Drug Delivery and Translational Research* **15**, 2924-2940 (2025).
14. Bu, L.-L. et al. in International Journal of Molecular Sciences, Vol. 24 15160 (2023).
15. Wang, Y., Chuang, C.Y., Hawkins, C.L. & Davies, M.J. in Antioxidants, Vol. 11 1616 (2022).
16. Wolosowicz, M., Prokopiuk, S. & Kaminski, T.W. in Pharmaceutics, Vol. 17 1425 (2025).
17. Baragetti, A. et al. Neutrophil aging exacerbates high fat diet induced metabolic alterations. *Metabolism - Clinical and Experimental* **144** (2023).
18. Pickett, J.R., Wu, Y., Zacchi, L.F. & Ta, H.T. Targeting endothelial vascular cell adhesion molecule-1 in atherosclerosis: drug discovery and development of vascular cell adhesion molecule-1–directed novel therapeutics. *Cardiovascular Research* **119**, 2278-2293 (2023).
19. Goswami, S.K., Ranjan, P., Dutta, R.K. & Verma, S.K. Management of inflammation in cardiovascular diseases. *Pharmacological Research* **173**, 105912 (2021).
20. Shen, J., Zhao, M., Zhang, C. & Sun, X. IL-1β in atherosclerotic vascular calcification: From bench to bedside. *International Journal of Biological Sciences* **17**, 4353-4364 (2021).
21. Hu, Y. et al. Co-Assembled Binary Polyphenol Natural Products for the Prevention and Treatment of Radiation-Induced Skin Injury. *ACS Nano* **18**, 27557-27569 (2024).
22. Chen, L. et al. Therapeutic potential of atorvastatin in ischemic stroke: an investigation into its anti-inflammatory effect by targeting the gut-brain axis. *Journal of Translational Medicine* **23**, 750 (2025).
23. Kanehisa, M., Furumichi, M., Sato, Y., Kawashima, M. & Ishiguro-Watanabe, M. KEGG for taxonomy-based analysis of pathways and genomes. *Nucleic Acids Research* **51**, D587-D592 (2023).
24. Kanehisa, M., Furumichi, M., Sato, Y., Matsuura, Y. & Ishiguro-Watanabe, M. KEGG: biological systems database as a model of the real world. *Nucleic Acids Research* **53**, D672-D677 (2025).

Acknowledgements: The authors thank the members of the Institute of Biomedical Engineering, Chinese Academy of Medical Science & Peking Union Medical College for their assistance.

Authors' contributions: Aiai Zhang and Kaijing Liu conceived the project and designed the experiments. Aiai Zhang, Yue Shi, Wei Liu, Feixing Li and Wei Han performed experiments and prepared the figures. Aiai Zhang analyzed and discussed the results. Aiai Zhang and

Meiling Du wrote the manuscript. Jing Yang, Wenqing Gao and Kaijing Liu reviewed and edited the manuscript. All authors have given approval to the final version of the manuscript.

Declarations

Competing interests: The authors declare no competing interests.

Ethics approval and consent to participate: Not applicable.

Consent for publication: Not applicable.

Funding: This study was supported by Hebei Natural Science Foundation (H2024405017), National Natural Science Foundation of China (82600821)and Shandong Provincial Natural Science Foundation (ZR2026QC1699).

Reprints and permissions information is available at www.nature.com/reprints.

Publisher's note Springer Nature remains neutral with regard to jurisdictional claims in published maps and institutional affiliations.

Open Access This article is licensed under a Creative Commons Attribution-NonCommercial-NoDerivatives 4.0 International License, which permits any non-commercial use, sharing, distribution and reproduction in any medium or format, as long as you give appropriate credit to the original author(s) and the source, provide a link to the Creative Commons licence, and indicate if you modified the licensed material. You do not have permission under this licence to share adapted material derived from this article or parts of it. The images or other third party material in this article are included in the article's Creative Commons licence, unless indicated otherwise in a credit line to the material. If material is not included in the article's Creative Commons licence and your intended use is not permitted by statutory regulation or exceeds the permitted use, you will need to obtain permission directly from the copyright holder. To view a copy of this licence, visit http://creativecommons.org/licenses/by-nc-nd/4.0/.

Supplementary Files

This is a list of supplementary files associated with this preprint. Click to download.

- ToC.png
- SI.pdf